Analytic derivative couplings and first-principles exciton/phonon coupling constants for an *ab initio* Frenkel-Davydov exciton model: Theory, implementation, and application to compute triplet exciton mobility parameters for crystalline tetracene

Adrian F. Morrison and John M. Herbert[a)]
Department of Chemistry and Biochemistry, The Ohio State University, Columbus, Ohio 43210, USA

(Received 1 April 2017; accepted 31 May 2017; published online 14 June 2017)

Recently, we introduced an *ab initio* version of the Frenkel-Davydov exciton model for computing excited-state properties of molecular crystals and aggregates. Within this model, supersystem excited states are approximated as linear combinations of excitations localized on molecular sites, and the electronic Hamiltonian is constructed and diagonalized in a direct-product basis of non-orthogonal configuration state functions computed for isolated fragments. Here, we derive and implement analytic derivative couplings for this model, including nuclear derivatives of the natural transition orbital and symmetric orthogonalization transformations that are part of the approximation. Nuclear derivatives of the exciton Hamiltonian's matrix elements, required in order to compute the nonadiabatic couplings, are equivalent to the "Holstein" and "Peierls" exciton/phonon couplings that are widely discussed in the context of model Hamiltonians for energy and charge transport in organic photovoltaics. As an example, we compute the couplings that modulate triplet exciton transport in crystalline tetracene, which is relevant in the context of carrier diffusion following singlet exciton fission. *Published by AIP Publishing.* [http://dx.doi.org/10.1063/1.4985607]

I. INTRODUCTION

In a variety of important chemical systems, the motion of nuclei can induce electronic transitions, which represents a breakdown of the Born-Oppenheimer approximation. This is well known in molecular photophysics and photochemistry,[1–4] including the photochemistry of biologically important molecules,[5,6] leading to vibronic effects in molecular spectroscopy,[4,7] including the Jahn-Teller effect.[8] Nonadiabatic effects are also important in nanoscale systems where they influence charge transport in organic photovoltaics,[9] charge recombination in photo-excited nanoparticles,[10] and singlet fission in crystalline organic materials,[11] processes that are challenging to model using quantum chemistry due to the size of the systems involved.

For molecular crystals and aggregates, a promising approach is an *ab initio* version of the Frenkel-Davydov exciton model that we have recently introduced.[12–14] In keeping with the original ideas of Frenkel[15] and Davydov,[16] the wave function for a (potentially) collective excitation is expanded in a basis consisting of direct products of monomer wave functions, one or more of which may be excited. However, unlike the early models (and even many recent ones, e.g., Refs. 17–20), we do not make any sort of dipole-coupling, nearest-neighbor, frontier orbital, neglect-of-exchange, or other approximations to the Hamiltonian for the full system. Exact Hartree-Fock Coulomb and exchange interactions are included, although a charge-embedding scheme for distant monomer units has been successfully employed to significantly reduce the cost.[13] Our *ab initio* Frenkel-Davydov exciton model (AIFDEM) reproduces supersystem excitation energies to within 0.1–0.2 eV for systems including DNA base pairs, crystalline acenes, aggregates of organic chromophores, and water clusters,[12,13] and we have demonstrated that supersystems containing the equivalent of more than 50 000 basis functions can be treated with modest hardware requirements.[12] The ability of this method to include a large number of monomers in the calculation allowed us to demonstrate that the signatures of quantum coherence in excitation energy transfer may persist to longer time scales as compared to those in smaller models that are accessible to traditional quantum chemistry calculations.[14]

Here, we report the derivation and implementation of analytic derivative couplings for this *ab initio* Frenkel-Davydov exciton model (AIFDEM). Namely, this means the first-order derivative couplings

$$\mathbf{d}^{JK} = \langle \Psi_J | \hat{\boldsymbol{\nabla}} | \Psi_K \rangle, \tag{1}$$

where Ψ_J and Ψ_K are adiabatic electronic states and $\hat{\boldsymbol{\nabla}}$ represents derivatives with respect to Cartesian coordinates of the nuclei. Derivative couplings codify the coupling of electronic states due to nuclear motion and can be said to drive nonadiabatic transitions. If the states Ψ_J and Ψ_K are exact eigenstates of the electronic Hamiltonian, $\hat{H}$, then it can be shown that

$$\mathbf{h}^{JK} = \left\langle \Psi_J \middle| \frac{\partial \hat{H}}{\partial \mathbf{x}} \middle| \Psi_K \right\rangle = (E_J - E_K)\, \mathbf{d}^{JK}. \tag{2}$$

The quantities $\mathbf{h}^{JK}$ are known as the nonadiabatic couplings, and they describe the topology around the conical intersections between adiabatic potential energy surfaces. Knowledge of $\mathbf{h}^{JK}$ facilitates the use of more efficient algorithms for

a)herbert@chemistry.ohio-state.edu

locating minimum-energy crossing points along conical seams between adiabatic electronic states.[21–23] Although the nonadiabatic couplings could be computed numerically,[24] an analytic implementation will be both more efficient and more accurate. For example, our group's implementation of $\mathbf{h}^{JK}$ at the level of configuration-interaction singles (CIS) and time-dependent density functional theory (TD-DFT) requires very little overhead on top of a CIS or TD-DFT gradient calculation.[23]

Some of the first derivations and computer implementation of first-order derivative couplings were done by Lengsfield, Yarkony, and co-workers for multi-reference CI and multi-reference self-consistent field models,[25–28] with new implementations as recently as 2016.[29] These quantities have also been derived at the level of equation-of-motion coupled-cluster theory.[30,31] Each of the aforementioned methods is potentially accurate yet expensive, so for extension to larger systems, the quantities $\mathbf{h}^{JK}$ have also been implemented for CIS wave functions,[23,32–34] spin-flip CIS wave functions,[23] and their TD-DFT analogues.[23,34–37] Nevertheless, the scaling of these methods remains $\mathcal{O}(N^4)$ with respect to system size. Moreover, the two-electron integral contraction required at each Davidson iteration, as well as iterative solution of the coupled-perturbed equations,[38] is challenging to implement efficiently on modern, massively parallel computer architectures. Furthermore, the single-excitation *ansatz* is incapable of treating highly correlated and multi-reference excited states, including the key multi-exciton intermediate in the singlet fission process.[39]

By exploiting localized basis states and charge embedding, the AIFDEM can, in principle, substantially reduce the cost of supersystem CIS or TD-DFT calculations in molecular crystals and aggregates and can qualitatively describe the *inter*molecular electron correlation that defines the aforementioned multi-exciton state. Here, we derive and implement computational expressions for the quantities $\mathbf{H}^{[x]}_{JK} = \langle \Psi_J | \partial \hat{H} / \partial x | \Psi_K \rangle$ for wave functions Ψ_J and Ψ_K obtained from the AIFDEM. The derivation requires expressions for the derivative of the transformation from canonical molecular orbitals (MOs) to natural transition orbitals (NTOs),[40–42] as well as the derivative of Löwdin's symmetric orthogonalization transformation. Notably, the resulting expressions for the derivative couplings $\mathbf{H}^{[x]}_{JK}$ involve intermediate quantities that are equivalent to the so-called "Holstein" and "Peierls" coupling constants that are routinely discussed in the literature on organic photovoltaics. Indeed, we have recently used the AIFDEM formalism to compute these exciton/phonon couplings from first principles for the process of singlet fission in crystalline tetracene,[43] but the details of the implementation are provided here for the first time. Finally, we use this formalism to compute the exciton/phonon coupling constants that modulate triplet exciton mobility in crystalline tetracene, quantities that are also relevant in the context of singlet fission.

II. THEORY

A. Notation

In what follows, we adopt the matrix formalism of Maurice and Head-Gordon,[44] where boldface symbols represent vector-, matrix-, or tensor-valued quantities, and manipulations of these objects then refer to linear algebra operations: **AB** indicates matrix multiplication and

$$\mathbf{A} \cdot \mathbf{B} = \sum_{mn} A_{mn} B_{mn}. \tag{3}$$

If **A** and/or **B** is symmetric, which will be the case here, then $\mathbf{A} \cdot \mathbf{B} = \mathrm{tr}(\mathbf{AB})$.

Molecular monomer units, whose total number we shall denote as F, are indexed as $A, B, \ldots$. Indices $i, j, \ldots$ and $a, b, \ldots$ refer to occupied and virtual MOs, respectively; $\mu, \nu \ldots$ refer to AOs; and τ is a spin index equal to α or β. The superscript $[x]$ will denote a partial derivative with respect to the nuclear coordinate x. Atomic units are used throughout.

B. Model

An exciton model describes a collective excitation of the supersystem as a linear combination of excitations that are localized on molecular sites. Formally, the excited states are linear combinations of "exciton-site" basis states, each consisting of a direct product of monomer wave functions wherein one fragment is excited. The collective wave function for the Ith excited state is thus

$$|\Xi^I\rangle = \sum_n K_{In} |\Psi_A \Psi_B \cdots \Psi^*_n \cdots \Psi_F\rangle. \tag{4}$$

The exciton-site basis also includes a ground-state configuration and can be expanded with more states to fit the problem at hand, e.g., by inclusion of charge-separated states $|\Psi^+_A \Psi^-_B \cdots \Psi_F\rangle$.[43] Coefficients K_{In} specify the contribution to eigenstate I of the supersystem that arises from the excitation of monomer n. These coefficients are determined by solving the generalized eigenvalue problem,

$$\mathbf{HK}_I = \epsilon_I \mathbf{SK}_I. \tag{5}$$

The quantities **H** and **S** are the AIFDEM electronic Hamiltonian and overlap matrices, respectively. The latter arises because the exciton-site basis states are not generally orthogonal, although the supersystem eigenstates are orthogonal, hence

$$\mathbf{K}^\dagger_I \mathbf{SK}_J = \delta_{IJ}. \tag{6}$$

We construct an exciton-site basis as direct products of configuration state functions (CSFs) computed for the isolated fragments. The ground-state basis function

$$|\Psi_A \Psi_B \cdots \Psi_F\rangle = |\Phi_A \Phi_B \cdots \Phi_F\rangle \tag{7}$$

is a direct product of determinants Φ_M for each monomer. Excited states are described at the CIS or TDDFT level (for the latter, within the Tamm-Dancoff approximation[45]) as linear combinations of singly-substituted determinants,

$$|\Psi^*_M\rangle = \sum_{ia} T^{ia} |\Phi^{ia}_M\rangle. \tag{8}$$

The CI amplitude T^{ia} codifies an occupied → virtual ($i \to a$) excitation.

A crucial aspect of our algorithm involves the transformation of the monomer MOs and amplitude matrix **T** into the basis of NTOs,[40–42] the latter of which are equivalent to CIS or TDDFT natural orbitals.[46] (This equivalence is a unique feature of single-substitution wave functions, whose natural

orbitals do not mix occupied and virtual orbitals; see Ref. 46.) This transformation reduces the number of terms in Eq. (8) to no more than the number of electrons on monomer M. Typically only a few of the transformed amplitudes are significant, and this number can be further truncated, in a controlled fashion, in order to preserve a certain threshold of the norm of the transition density. The NTOs comprise corresponding occupied/virtual pairs; hence, the dual indices ia are redundant upon transformation, and we can safely denote the CI amplitudes in the NTO basis as t^i rather than T^{ia}. A singly-excited, direct-product basis function can then be expressed as, e.g.,

$$|\Psi_A^* \Psi_B \cdots \Psi_F\rangle = \sum_{i\in A} t^i \, |\Phi_A^i \Phi_B \cdots \Phi_F\rangle, \tag{9}$$

bearing in mind that $|\Phi_A^i\rangle$ might need to be a CSF rather than a single Slater determinant, in order to obtain correct spin symmetry.[43]

C. Matrix elements

We require matrix elements of $\hat{H}$ in the basis of Eq. (9),

$$\begin{aligned} H_{AB} &= \langle \Psi_A^* \Psi_B \cdots \Psi_F | \hat{H} | \Psi_A \Psi_B^* \cdots \Psi_F \rangle \\ &= \sum_{i\in A} \sum_{j\in B} t^i \, t^j \, \langle \Phi_A^i \Phi_B \cdots \Phi_F | \hat{H} | \Phi_A \Phi_B^j \cdots \Phi_F \rangle, \end{aligned} \tag{10}$$

as well as the corresponding overlap matrix elements

$$\begin{aligned} S_{AB} &= \langle \Psi_A^* \Psi_B \cdots \Psi_F | \Psi_A \Psi_B^* \cdots \Psi_F \rangle \\ &= \sum_{i\in A} \sum_{j\in B} t^i \, t^j \, \langle \Phi_A^i \Phi_B \cdots \Phi_F | \Phi_A \Phi_B^j \cdots \Phi_F \rangle. \end{aligned} \tag{11}$$

For each of the terms in Eqs. (10) and (11), the bra and ket sets of orbitals are symmetrically orthogonalized among themselves and expanded in a common AO basis. The orbitals can then be represented as a matrix, for instance, the columns of $\mathbf{C}^i$ contain the coefficients for the orthogonalized orbitals of $|\Phi_A^i \Phi_B \cdots \Phi_F\rangle$. To compute the matrix elements between the two sets of orbitals, which are not orthogonal, we use the corresponding orbitals transformation and generalized Slater-Condon rules.[47,48] Note that the corresponding orbitals transformation requires the sets of orbitals of different spins to be treated individually. For simplicity, we will suppress spin indices on expressions treating a single spin and include a spin index only when quantities involving both spin cases are needed.

We proceed by defining an AO overlap matrix $\mathbf{s}$,

$$s_{\mu\nu} = \langle \mu | \nu \rangle \tag{12}$$

and then form the MO overlap matrix

$$\mathbf{S}^{ij} = (\mathbf{C}^i)^\dagger \, \mathbf{s} \, \mathbf{C}^j \tag{13}$$

using the bra and ket orbitals (of a single spin) from a given term in Eq. (10) or (11). We then compute the singular value decomposition (SVD) of $\mathbf{S}^{ij}$,

$$\mathbf{S}^{ij} = \mathbf{U}^{ij} \boldsymbol{\lambda}^{ij} (\mathbf{V}^{ij})^\dagger, \tag{14}$$

which is defined by the diagonal matrix $\boldsymbol{\lambda}^{ij}$ of singular values and by the unitary matrices $\mathbf{U}^{ij}$ and $\mathbf{V}^{ij}$. A generalized density matrix

$$\mathbf{G}^{ij} = \mathbf{C}^j \mathbf{V}^{ij} \left(\boldsymbol{\lambda}^{ij}\right)^{-1} (\mathbf{U}^{ij})^\dagger (\mathbf{C}^i)^\dagger \tag{15}$$

can then be formed from the transformed MOs, and we introduce the quantity

$$\begin{aligned} \xi^{ij} &= \det[\mathbf{U}^{ij} (\mathbf{V}^{ij})^\dagger] \, \det(\boldsymbol{\lambda}^{ij}) \\ &= \Upsilon^{ij} \, \det(\boldsymbol{\lambda}^{ij}), \end{aligned} \tag{16}$$

which is a scalar that will ensure consistent norm and phase. [Note that since $\boldsymbol{\lambda}^{ij}$ is diagonal, $\det(\boldsymbol{\lambda}^{ij})$ is simply the product of the singular values.] This equation also serves to define $\Upsilon^{ij} = \det[\mathbf{U}^{ij} (\mathbf{V}^{ij})^\dagger]$.

Finally, we can write simple expressions for the overlap matrix elements,

$$S_{AB} = \sum_{i\in A} \sum_{j\in B} t^i \, t^j \, \xi_\alpha^{ij} \, \xi_\beta^{ij} \tag{17}$$

and for the matrix elements of the Hamiltonian,

$$H_{AB} = \sum_{i\in A} \sum_{j\in B} t^i \, t^j \, \xi_\alpha^{ij} \, \xi_\beta^{ij} \, \Gamma^{ij}. \tag{18}$$

In the latter equation,

$$\begin{aligned} \Gamma^{ij} = {} & (\mathbf{G}_\alpha^{ij} + \mathbf{G}_\beta^{ij}) \cdot \mathbf{h} + \tfrac{1}{2} \mathbf{G}_\alpha^{ij} \cdot \boldsymbol{\Pi} \cdot \mathbf{G}_\alpha^{ij} \\ & + \mathbf{G}_\beta^{ij} \cdot \boldsymbol{\Pi} \cdot \mathbf{G}_\beta^{ij} + \mathbf{G}_\alpha^{ij} \cdot \boldsymbol{\Pi}^\circ \cdot \mathbf{G}_\beta^{ij}. \end{aligned} \tag{19}$$

The quantities ξ_τ^{ij} in Eqs. (17) and (18), and $\mathbf{G}_\tau^{ij}$ in Eq. (19), are built from orbitals and transformation matrices having a spin index $\tau \in \{\alpha, \beta\}$. The quantity $\mathbf{h}$ in Eq. (19) is the core Hamiltonian, and the four-index tensor $\boldsymbol{\Pi}$ contains antisymmetrized electron repulsion integrals,

$$\Pi_{\mu\nu\lambda\sigma} = \langle \mu\nu || \lambda\sigma \rangle, \tag{20}$$

while $\boldsymbol{\Pi}^\circ$ contains Coulomb integrals,

$$\Pi^\circ_{\mu\nu\lambda\sigma} = \langle \mu\nu | \lambda\sigma \rangle. \tag{21}$$

The latter arise in Eq. (19) because the exchange integrals vanish for the mixed-spin term.

In some cases, one or more of the singular values in $\boldsymbol{\lambda}^{ij}$ might approach zero, potentially leading to singularities in $\mathbf{G}^{ij}$. The algorithm is then modified to use special case co-density matrices such that the generalized Slater-Condon rules are recovered. Such a procedure is described in Ref. 49.

D. Derivative couplings

We seek to compute the first-order derivative couplings $\mathbf{d}^{JK}$ for the AIFDEM. As our model is essentially a form of non-orthogonal CI, we can adopt the general procedure that was derived by Lengsfield, Yarkony, and co-workers in the context of CI wave functions built upon a MCSCF reference state.[27] (The same approach has also been adapted to compute derivative couplings for CIS, TD-DFT, and their spin-flip analogues.[23,32]) Applying the chain rule to Eq. (4) and acting from the left with $\langle \Xi_J |$, we obtain

$$\langle \Xi_J | (\partial/\partial x) | \Xi_I \rangle = \mathbf{K}_J^\dagger \mathbf{S} \mathbf{K}_I^{[x]} + \mathbf{K}_J^\dagger \mathbf{S}^{\mathrm{R}[x]} \mathbf{K}_I. \tag{22}$$

The quantity $\mathbf{S}^{\mathrm{R}[x]}$ is the right overlap derivative matrix in the exciton-site basis,

$$S_{AB}^{\mathrm{R}[x]} = \langle \Psi_A^* \Psi_B \cdots \Psi_F | (\Psi_A \Psi_B^* \cdots \Psi_F)^{[x]} \rangle. \tag{23}$$

In order to eliminate the coefficient derivatives, $\mathbf{K}_I^{[x]}$, we differentiate the eigenvalue problem in Eq. (5) and left-multiply by $\mathbf{K}_J^\dagger$,

$$\mathbf{K}_J^\dagger \mathbf{H}^{[x]} \mathbf{K}_I + \mathbf{K}_J^\dagger \mathbf{H} \mathbf{K}_I^{[x]} = \epsilon_I^{[x]} \mathbf{K}_J^\dagger \mathbf{S} \mathbf{K}_I + \epsilon_I \mathbf{K}_J^\dagger \mathbf{S}^{[x]} \mathbf{K}_I + \epsilon_I \mathbf{K}_J^\dagger \mathbf{S} \mathbf{K}_I^{[x]}. \quad (24)$$

Here, $\mathbf{S}^{[x]}$ is the symmetric overlap matrix derivative in the exciton-site basis,

$$S_{AB}^{[x]} = \langle (\Psi_A^* \Psi_B \cdots \Psi_F)^{[x]} | \Psi_A \Psi_B^* \cdots \Psi_F \rangle + \langle \Psi_A^* \Psi_B \cdots \Psi_F | (\Psi_A \Psi_B^* \cdots \Psi_F)^{[x]} \rangle. \quad (25)$$

By acting to the left with $\mathbf{H}$ in the second term on the left side of Eq. (24), and using the orthogonality of the eigenstates to eliminate the first term on the right, we obtain after some rearrangement

$$\mathbf{K}_J^\dagger \mathbf{S} \mathbf{K}_I^{[x]} = \frac{\mathbf{K}_J^\dagger \mathbf{H}^{[x]} \mathbf{K}_I - \epsilon_I \mathbf{K}_J^\dagger \mathbf{S}^{[x]} \mathbf{K}_I}{(\epsilon_I - \epsilon_J)}. \quad (26)$$

Finally, Eq. (26) can then be inserted into Eq. (22) to afford

$$\langle \Xi_J | (\partial/\partial x) | \Xi_I \rangle = \frac{\mathbf{K}_J^\dagger \mathbf{H}^{[x]} \mathbf{K}_I - \epsilon_I \mathbf{K}_J^\dagger \mathbf{S}^{[x]} \mathbf{K}_I}{(\epsilon_I - \epsilon_J)} + \mathbf{K}_J^\dagger \mathbf{S}^{\mathrm{R}[x]} \mathbf{K}_I. \quad (27)$$

The term involving $\mathbf{K}_J^\dagger \mathbf{H}^{[x]} \mathbf{K}_I$ is the familiar Hellman-Feynman expression for derivative couplings, and the other two terms are analogous to the Pulay terms that arise in SCF gradient theory using atom-centered basis functions. We identify the term $\mathbf{K}_J^\dagger \mathbf{H}^{[x]} \mathbf{K}_I$ in Eq. (27) as the nonadiabatic coupling, as established in the context of multireference CI and adopted by others.[23]

E. Derivatives of the matrix elements

To evaluate either the nonadiabatic coupling, the derivative coupling, or the energy gradient, we need $\mathbf{H}^{[x]}$, the derivative of the Hamiltonian in the exciton-site basis. Derivatives of the matrix elements are given by

$$H_{AB}^{[x]} = \sum_{i \in A} \sum_{j \in B} (t^i t^j \xi_\alpha^{ij} \xi_\beta^{ij})^{[x]} \Gamma^{ij} + t^i t^j \xi_\alpha^{ij} \xi_\beta^{ij} \Gamma^{ij[x]}, \quad (28)$$

where

$$\Gamma^{ij[x]} = (\mathbf{G}_\alpha^{ij} + \mathbf{G}_\beta^{ij})^{[x]} \cdot \mathbf{h} + (\mathbf{G}_\alpha^{ij} + \mathbf{G}_\beta^{ij}) \cdot \mathbf{h}^{[x]} + \mathbf{G}_\alpha^{ij[x]} \cdot \mathbf{\Pi} \cdot \mathbf{G}_\alpha^{ij} + \mathbf{G}_\beta^{ij[x]} \cdot \mathbf{\Pi} \cdot \mathbf{G}_\beta^{ij} + \mathbf{G}_\alpha^{ij[x]} \cdot \mathbf{\Pi}^\circ \cdot \mathbf{G}_\beta^{ij} + \mathbf{G}_\alpha^{ij} \cdot \mathbf{\Pi}^\circ \cdot \mathbf{G}_\beta^{ij[x]} + \tfrac{1}{2} \mathbf{G}_\alpha^{ij} \cdot \mathbf{\Pi}^{[x]} \cdot \mathbf{G}_\alpha^{ij} + \tfrac{1}{2} \mathbf{G}_\beta^{ij} \cdot \mathbf{\Pi}^{[x]} \cdot \mathbf{G}_\beta^{ij} + \mathbf{G}_\alpha^{ij} \cdot \mathbf{\Pi}^{[x]\circ} \cdot \mathbf{G}_\beta^{ij}. \quad (29)$$

The quantities $\mathbf{h}^{[x]}$ and $\mathbf{\Pi}^{[x]}$ are one- and two-electron integral derivatives, as required also to evaluate the SCF gradient, and $\mathbf{\Pi}^{[x]\circ}$ again indicates Coulomb integrals only. The expression in Eq. (29) takes advantage of symmetries such as

$$\mathbf{G}^{ij[x]} \cdot \mathbf{\Pi} \cdot \mathbf{G}^{ij} = \mathbf{G}^{ij} \cdot \mathbf{\Pi} \cdot \mathbf{G}^{ij[x]}. \quad (30)$$

However, when non-coincidences occur in the corresponding orbitals, necessitating the use of co-densities,[49] Eq. (30) is no longer valid, and the terms on the left and the right in Eq. (30) must be computed explicitly.

The required derivatives of the generalized density matrices, $\mathbf{G}^{ij[x]}$, can be obtained by direct differentiation of Eq. (15) with the result

$$\mathbf{G}^{ij[x]} = \mathbf{C}^{j[x]} \mathbf{V}^{ij} \left(\boldsymbol{\lambda}^{ij}\right)^{-1} (\mathbf{U}^{ij})^\dagger (\mathbf{C}^i)^\dagger + \mathbf{C}^j \mathbf{V}^{ij[x]} (\boldsymbol{\lambda}^{ij})^{-1} (\mathbf{U}^{ij})^\dagger (\mathbf{C}^i)^\dagger + \mathbf{C}^j \mathbf{V}^{ij} [(\boldsymbol{\lambda}^{ij})^{-1}]^{[x]} (\mathbf{U}^{ij})^\dagger (\mathbf{C}^i)^\dagger + \mathbf{C}^j \mathbf{V}^{ij} (\boldsymbol{\lambda}^{ij})^{-1} (\mathbf{U}^{ij[x]})^\dagger (\mathbf{C}^i)^\dagger + \mathbf{C}^j \mathbf{V}^{ij} (\boldsymbol{\lambda}^{ij})^{-1} (\mathbf{U}^{ij})^\dagger (\mathbf{C}^{i[x]})^\dagger. \quad (31)$$

Derivatives $\mathbf{U}^{ij[x]}$, $\mathbf{V}^{ij[x]}$, and $\boldsymbol{\lambda}^{ij[x]}$ of the matrices that define the SVD are required in Eq. (31), expressions for which can be found in the mathematics literature.[50,51] (For completeness, the algorithm used to compute the SVD derivative is provided in the Appendix.) These expressions depend on the derivative of the MO overlap matrix as defined in Eq. (14), which is

$$\mathbf{S}^{ij[x]} = \mathbf{C}^{i[x]} \mathbf{s} \mathbf{C}^j + \mathbf{C}^i \mathbf{s}^{[x]} \mathbf{C}^j + \mathbf{C}^i \mathbf{s} \mathbf{C}^{j[x]}, \quad (32)$$

in which $\mathbf{s}^{[x]}$ is the derivative of the AO overlap matrix. Along with $\mathbf{h}^{[x]}$ and $\mathbf{\Pi}^{[x]}$, $\mathbf{s}^{[x]}$ is a standard quantity in SCF gradient theory.

Using these quantities, the derivative of the phase and normalization constants $\xi^{ij[x]}$ defined in Eq. (28) can be evaluated by differentiating Eq. (16). Using the definition of the derivative of a determinant, and taking advantage of the fact that $\mathbf{U}^{ij}$ and $\mathbf{V}^{ij}$ are unitary, one obtains

$$\xi^{ij[x]} = \Upsilon^{ij} \mathbf{U}^{ij\dagger} \mathbf{V}^{ij} (\mathbf{U}^{ij[x]} \mathbf{V}^{ij\dagger} + \mathbf{U}^{ij} \mathbf{V}^{ij[x]\dagger}) (\det \boldsymbol{\lambda}^{ij}) + \Upsilon^{ij} (\det \boldsymbol{\lambda}^{ij})^{[x]}. \quad (33)$$

The final derivative in this equation, $(\det \boldsymbol{\lambda}^{ij})^{[x]}$, is equal to the derivative of the product of the singular values. Expressions for derivatives of singular values are given in Refs. 50 and 51 and in the Appendix.

We now turn to the MO coefficient derivatives, $\mathbf{C}^{i[x]}$. Since the MOs are computed for isolated fragments, their canonical derivatives are also computed at the fragment level by solving coupled-perturbed (CP)-SCF equations,[52] much like computing a SCF Hessian. Note that only fragment-level CP-SCF equations are ever required, and the coefficient derivatives for a particular fragment vanish if the nuclear coordinate x does not belong to that fragment. It is possible that the Handy-Schaefer Z-vector technique[53] could be used to avoid solving CP-SCF equations for each perturbation x, though this is potentially complicated by the fact that the orbital coefficients that appear in Eqs. (15) and (31) are not in the canonical basis, but rather have been transformed into the NTO basis and then symmetrically orthogonalized. (Derivatives of these transformations are derived below.) Moreover, the main bottleneck in AIFDEM derivative coupling calculations is contraction of integral derivatives with densities, so that the Z-vector technique would likely afford a modest reduction in the overall cost.

F. Derivatives of the NTO transformation

Derivatives of the matrices that define the transformation from canonical MOs to NTOs have not been reported previously but are fairly straightforward. NTOs are formed from

separate unitary transformations of the occupied and the virtual MOs,

$$\bar{\mathbf{C}}_{\mathrm{O}} = \widetilde{\mathbf{C}}_{\mathrm{O}}\mathbf{O}, \tag{34a}$$

$$\bar{\mathbf{C}}_{\mathrm{V}} = \widetilde{\mathbf{C}}_{\mathrm{V}}\mathbf{N}. \tag{34b}$$

Tildes indicate canonical MO coefficients and overbars denote NTO coefficients. For the AIFDEM, the NTO transformation is performed separately on each fragment. The unitary matrices **O** and **V** arise from the SVD of the matrix **T** of single-particle transition amplitudes,

$$\mathbf{t} = \mathbf{O}\mathbf{T}\mathbf{N}^{\dagger}, \tag{35}$$

in which **t** is diagonal.

Differentiating Eq. (34) affords

$$\bar{\mathbf{C}}_{\mathrm{O}}^{[x]} = \widetilde{\mathbf{C}}_{\mathrm{O}}\mathbf{O}^{[x]} + \widetilde{\mathbf{C}}_{\mathrm{O}}^{[x]}\mathbf{O}, \tag{36a}$$

$$\bar{\mathbf{C}}_{\mathrm{V}}^{[x]} = \widetilde{\mathbf{C}}_{\mathrm{V}}\mathbf{N}^{[x]} + \widetilde{\mathbf{C}}_{\mathrm{V}}^{[x]}\mathbf{N}. \tag{36b}$$

Derivatives $\mathbf{O}^{[x]}$ and $\mathbf{N}^{[x]}$ of the transformation matrices require again the application of the SVD differentiation algorithm, albeit in an entirely different context as compared to Eq. (31). This will also return the CI amplitude derivatives $\mathbf{t}^{[x]}$ expressed in the NTO basis. As an input, the SVD differentiation requires **T** and the canonical amplitude derivatives, $\mathbf{T}^{[x]}$, which are found by solving coupled-perturbed CIS equations on the isolated fragments.[38] Like the MO coefficient derivatives, only fragment level coupled-perturbed equations are required, and the amplitude derivative is zero if the coordinate x is outside of the fragment in question.

G. Derivatives of the symmetric orthogonalization transformation

To yield the final form of the orbital coefficient derivatives needed in Eq. (31), we require the derivative of the symmetric (Löwdin) orthogonalization transformation, which to the best of our knowledge has not been previously reported. The transformation in question is

$$\mathbf{C}^{i} = \bar{\mathbf{C}}^{i}(\mathbf{S}^{i})^{-1/2}, \tag{37}$$

where

$$\mathbf{S}^{i} = \bar{\mathbf{C}}^{i}\mathbf{s}\bar{\mathbf{C}}^{i} \tag{38}$$

is the overlap among the set of orbitals. The required derivative is simply

$$\mathbf{C}^{i[x]} = \bar{\mathbf{C}}^{i[x]}(\mathbf{S}^{i})^{-1/2} + \bar{\mathbf{C}}^{i}[(\mathbf{S}^{i})^{-1/2}]^{[x]}, \tag{39}$$

where the overbars represent non-orthogonal orbitals and their derivatives. Differentiating the condition

$$(\mathbf{S}^{i})^{-1/2}(\mathbf{S}^{i})^{1/2} = \mathbf{1} \tag{40}$$

and rearranging, we obtain

$$[(\mathbf{S}^{i})^{-1/2}]^{[x]} = -(\mathbf{S}^{i})^{-1/2}[(\mathbf{S}^{i})^{1/2}]^{[x]}(\mathbf{S}^{i})^{-1/2}. \tag{41}$$

In order to determine $[(\mathbf{S}^{i})^{1/2}]^{[x]}$, we differentiate the identity $\mathbf{S}^{i} = (\mathbf{S}^{i})^{1/2}(\mathbf{S}^{i})^{1/2}$ to obtain

$$\mathbf{S}^{i[x]} = [(\mathbf{S}^{i})^{1/2}]^{[x]}(\mathbf{S}^{i})^{1/2} + (\mathbf{S}^{i})^{1/2}[(\mathbf{S}^{i})^{1/2}]^{[x]}, \tag{42}$$

where

$$\mathbf{S}^{i[x]} = \bar{\mathbf{C}}^{i[x]}\mathbf{s}\bar{\mathbf{C}}^{i} + \bar{\mathbf{C}}^{i}\mathbf{s}^{[x]}\bar{\mathbf{C}}^{i} + \bar{\mathbf{C}}^{i}\mathbf{s}\bar{\mathbf{C}}^{i[x]}. \tag{43}$$

Equation (42) takes the well-known form of a Sylvester equation, or more specifically a Lyapunov equation, solvers for which are available in many linear algebra packages. By solving Eq. (42) for $[(\mathbf{S}^{i})^{1/2}]^{[x]}$ and using the result from Eq. (41), the desired derivative is obtained.

H. Vibronic Hamiltonian and exciton/phonon couplings

Derivative couplings are of course useful for describing crossings of adiabatic potential surfaces, and in the case of organic (molecular) semiconductors, they also describe the influence of phonons and intramolecular vibrational modes on exciton or charge-carrier mobilities, a crucial aspect of energy transfer.[9] This requires a somewhat different approach as compared to methods designed to simulate nonadiabatic dynamics in finite molecular systems.

The Holstein-Peierls vibronic Hamiltonian is a popular way to understand energy transfer organic photovoltaic materials, which successfully reproduces experimental carrier mobilities in a variety of systems.[54–57] The model consists of molecular sites $A, B, \ldots$ with site energies $E_A, E_B, \ldots$ and electronic couplings ("transfer integrals"[9]) V_{AB}, all of which are modulated by a collection of harmonic vibrations, as would seem appropriate for a crystalline environment. The vibronic Hamiltonian is

$$\hat{\mathcal{H}} = \sum_{A}\left[E_A + \sum_{\theta}\tfrac{1}{2}(\dot{q}_\theta^2 + \omega_\theta^2 q_\theta^2) + g_{AA\theta}\,q_\theta\right]\hat{a}_A^{\dagger}\hat{a}_A + \sum_{A}\sum_{B}\left(V_{AB} + \sum_{\theta} g_{AB\theta}\,q_\theta\right)\hat{a}_A^{\dagger}\hat{a}_B, \tag{44}$$

where operators $\hat{a}_A^{\dagger}$ and $\hat{a}_A$ create and annihilate an excitation, respectively, on site A, and the parameters $g_{AA\theta}$ and $g_{AB\theta}$ are exciton/phonon coupling constants. Couplings $g_{AA\theta}$ are said to be of "Holstein" or "local" type and quantify how the site energy E_A changes along the dimensionless normal mode coordinate q_θ, whereas "Peierls" or "non-local" couplings $g_{AB\theta}$ quantify the changes in the intersite couplings. (Vibrations could be treated quantum-mechanically by replacing q_θ and $\dot{q}_\theta$ with the appropriate operators, as we did in a recent quantum dynamics simulation of singlet fission in crystalline tetracene that demonstrated the importance of vibronic coupling in driving that process.[43])

In practice, the site energies E_A are often approximated as the HOMO energies of the monomers and the transfer integrals V_{AB} as HOMO/LUMO couplings.[9] Exciton/phonon couplings have usually been computed numerically via finite difference of the site energies and transfer integrals,[58] with variances sampled over molecular dynamics trajectories,[59] or else back-computed from relaxation energies.[57,60] Often it is only practical to compute couplings for just a few modes. Up to constants, however, the exciton/phonon couplings $g_{AA\theta}$ and $g_{AB\theta}$ in Eq. (44) are simply derivatives of H_{AA} and H_{AB} with respect to q_θ. Herein, we will compute these couplings for the unit cell of tetracene, for all of the vibrational modes q_θ.

To do this, we must first transform the non-orthogonal AIFDEM Hamiltonian derivatives to an orthogonal basis, $H_{AB}^{[x]} \rightarrow D_{AB}^{[x]}$, including the derivative of the orthogonalization transformation. For the latter, we use the symmetric orthogonalization derivative derived in Eq. (41), with $\mathbf{S}^{i}$ replaced by

the AIFDEM overlap matrix **S** from Eq. (5). Following this, only a simple coordinate transformation is required,

$$g_{AB\theta} = (2\mu_\theta\omega_\theta)^{-1/2} \sum_x D^{[x]}_{AB} L_{x\theta}. \tag{45}$$

The matrix **L** is the transformation whose column θ contains the normalized Cartesian displacements corresponding to q_θ. This mode has frequency ω_θ and effective mass μ_θ, whose inverse is defined by[61]

$$\mu_\theta^{-1} = \sum_x L^2_{x\theta}. \tag{46}$$

In some literature, the factor of $2^{-1/2}$ in Eq. (45) is folded into the coordinate transformation **L**; we follow the convention used in Ref. 62. Exciton/phonon couplings in this work have dimensions of energy.

I. Implementation and computational scaling

AIFDEM derivatives were implemented in a locally modified version of Q-Chem[63] and will be available in the v. 5.0 release. The entire AIFDEM framework, including the derivatives, is implemented following an object-oriented strategy that simplifies addition of new types of basis states, e.g., the charge-transfer states that were included in the singlet fission calculations in Ref. 43. As shown in Table I for a particular displacement of He_4 (treated as a pair of He_2 fragments, as shown in Fig. 1), analytic derivative results for $H^{[x]}_{AB}$ agree with finite-difference results to within $\sim 10^{-6}$ a.u. in each individual matrix element. Note that because the basis-state orbitals are arbitrary up to phase, the sign of the matrix elements is not guaranteed to be consistent for all displacement steps when numerical differentiation is employed. This necessitates cumbersome sign-matching schemes. A benefit of analytic derivatives is that the relative signs of the matrix element derivatives remain consistent and meaningful.

TABLE I. Derivatives $H^{[x]}_{MN}$ of the Hamiltonian matrix elements and derivatives $S^{[x]}_{MN}$ of the overlap matrix elements, for three different basis states M and N for $(He_2)_2$, using the aug-cc-pVTZ basis set. All NTOs were retained in these calculations, and the SCF and CIS convergence thresholds were both set to 10^{-10} a.u. while the integral screening threshold was 10^{-14} a.u. The finite-difference calculations used a five-point stencil central difference with displacements of 10^{-4} Å. (The particular displacement x is shown in Fig. 1.)

$H^{[x]}_{MN}$ absolute finite difference			
	$\|\Psi_A\Psi_B\rangle$	$\|\Psi^*_A\Psi_B\rangle$	$\|\Psi_A\Psi^*_B\rangle$
$\|\Psi_A\Psi_B\rangle$	0.027 254	0.024 589	0.015 125
$\|\Psi^*_A\Psi_B\rangle$	0.024 589	0.048 970	0.004 776
$\|\Psi_A\Psi^*_B\rangle$	0.015 125	0.004 776	0.026 642
$H^{[x]}_{MN}$ analytic derivative			
	$\|\Psi_A\Psi_B\rangle$	$\|\Psi^*_A\Psi_B\rangle$	$\|\Psi_A\Psi^*_B\rangle$
$\|\Psi_A\Psi_B\rangle$	0.027 254	−0.024 589	−0.015 125
$\|\Psi^*_A\Psi_B\rangle$	−0.024 589	−0.048 970	−0.004 776
$\|\Psi_A\Psi^*_B\rangle$	−0.015 125	−0.004 776	0.026 642
$S^{[x]}_{MN}$ absolute finite difference			
	$\|\Psi_A\Psi_B\rangle$	$\|\Psi^*_A\Psi_B\rangle$	$\|\Psi_A\Psi^*_B\rangle$
$\|\Psi_A\Psi_B\rangle$	0.000 000	0.002 105	0.001 213
$\|\Psi^*_A\Psi_B\rangle$	−0.002 105	0.000 047	0.000 489
$\|\Psi_A\Psi^*_B\rangle$	−0.001 213	0.000 489	0.000 062
$S^{[x]}_{MN}$ analytic derivative			
	$\|\Psi_A\Psi_B\rangle$	$\|\Psi^*_A\Psi_B\rangle$	$\|\Psi_A\Psi^*_B\rangle$
$\|\Psi_A\Psi_B\rangle$	0.000 000	0.002 105	0.001 213
$\|\Psi^*_A\Psi_B\rangle$	0.002 105	−0.000 046	0.000 489
$\|\Psi_A\Psi^*_B\rangle$	0.001 213	0.000 489	−0.000 062

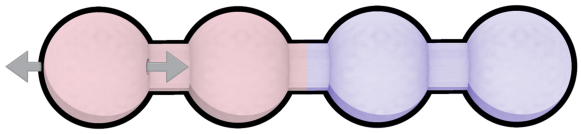

FIG. 1. Nuclear displacement of He_4 that is considered for the comparisons against finite-difference results in Table I. The two colors indicate how the system is divided up into a pair of He_2 fragments.

Computation of $H^{[x]}_{AB}$ in Eq. (28) has three potentially expensive steps. Recognizing that contractions of the form $\mathbf{F}^{ij} = \mathbf{\Pi} \cdot \mathbf{G}^{ij}$ are the primary bottleneck in energy calculations using the original AIFDEM,[12] we expect the analogous contractions $\mathbf{F}^{ij[x]} = \mathbf{\Pi}^{[x]} \cdot \mathbf{G}^{ij}$ to be a second potential bottleneck. Formation of $\mathbf{G}^{ij[x]}$ [Eq. (31)] is also a potential bottleneck; the cost of this step is dominated by the cost of evaluating the SVD derivative.

The total time for an AIFDEM derivative calculation and the contributions from these components for linear chains of He_2 fragments are shown in Fig. 2, for two different AO

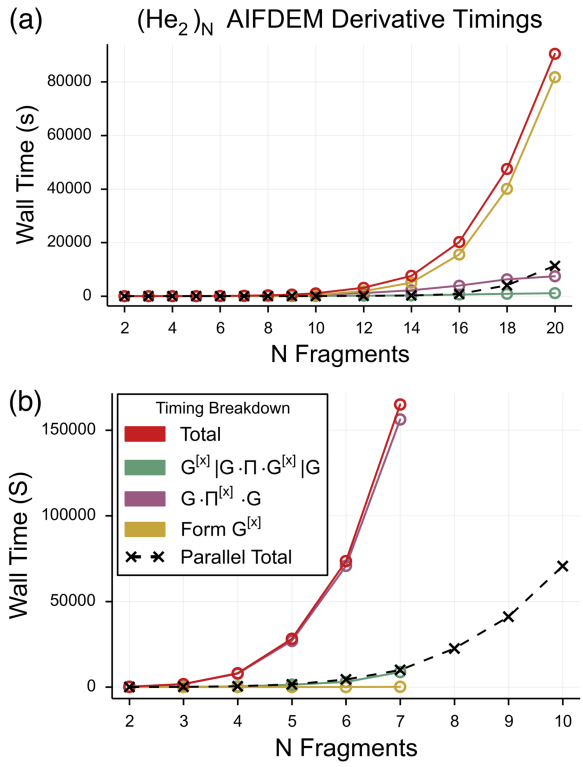

FIG. 2. Timing breakdown for derivative coupling calculations in linear helium chains in the (a) 6-311G and (b) aug-cc-pVTZ basis sets, retaining all NTOs in each case. All timings are measured on dual-socket Xeon E5-2680 v4 nodes with 128 GB of memory. Timing breakdowns are run in serial while parallel calculations use 28 cores.

basis sets. Unlike an AIFDEM energy calculation, for calculating derivatives, the cost to construct $\mathbf{F}^{ij}$ is a negligible fraction of the total cost, as our algorithm reuses these intermediates so that they do not need to be computed for each coordinate x. The bottleneck step is different in the two basis sets, switching from the formation of $\mathbf{G}^{ij[x]}$ (6-311G) to the contraction to form $\mathbf{F}^{ij[x]}$ (aug-cc-pVTZ). This is in line with expectations as the former step formally scales as $\mathcal{O}(N_{\text{occ}}^4)$ and the latter (in the absence of integral screening) as $\mathcal{O}(N_{\text{basis}}^4)$, so that the contraction to form $\mathbf{F}^{ij[x]}$ will dominate when $N_{\text{basis}} \gg N_{\text{occ}}$. For a more realistic system, namely, tetracene dimer in a 6-31+G* basis, about 14% of the cost comes from forming $\mathbf{G}^{ij[x]}$ and about 86% from forming $\mathbf{F}^{ij[x]}$.

In a standard AIFDEM derivative calculation, the derivative of each matrix element H_{AB} must be evaluated for each atomic coordinate x, which is approximately $3N_{\text{atom}}N_{\text{frag}}^2$ matrix elements. Each of these calculations is entirely independent, however, and can therefore be parallelized trivially and with unit efficiency. Our algorithm parallelizes matrix elements such that derivatives for the three Cartesian coordinates on a single nucleus are computed in a single batch assigned to one core. Including a greater number of $H_{AB}^{[x]}$ in a batch could potentially increase the efficiency of integral derivative evaluation at the expense of reduced parallelism; this is a potential means of optimization to be explored in the future. Shared-memory parallelization is accomplished using the message passing interface (MPI), with dynamic load balancing, and a parallel performance on a 28-core node is demonstrated for helium chains in Fig. 2. Parallel speedup is nearly ideal, and this excellent performance allows us to treat moderately sized systems easily, with adequate basis sets.

III. COMPUTATIONAL DETAILS

A. Tetracene crystal structure and phonon modes

Plane-wave DFT calculations to obtain the phonon spectrum of tetracene were performed using the Quantum Espresso package.[64] Variable unit cell optimization was performed, starting from the experimental crystal structure,[65,66] under 1 atm of pressure. As in our previous work on tetracene,[43] calculations were performed using the local density approximation (LDA) and norm-conserving pseudopotentials, with an SCF convergence threshold of 10^{-9} a.u., mixing parameter $\beta = 0.7$, and kinetic energy cutoff of 60 Ry (=120 hartree) for the plane-wave (PW) basis. The Brillouin zone was sampled using a $2 \times 2 \times 1$ k-point mesh, and phonon modes were then computed for this optimized structure at the Γ point.

As noted by Abdulla *et al.*,[67] lack of support for dispersion-corrected functionals for phonon calculations presents a major obstacle for studies of conjugated organic systems. A workaround is to forgo the use of a generalized gradient approximation in favor of LDA, as the latter has a tendency to overestimate binding energies, thereby compensating for the absence of attractive dispersion interactions. This is the approach that we take, and our computed phonon modes are in good agreement with those reported in Ref. 67.

B. Exciton model and derivatives

AIFDEM calculations were performed on an asymmetric tetracene dimer extracted from the DFT-optimized crystal structure, which constitutes the unit cell for crystalline tetracene. Exciton-site basis states, Eqs. (7) and (9), were constructed from fragment wave functions computed at the Hartree-Fock and CIS levels. AIFDEM calculations for the excited states and AIFDEM derivative calculations used a threshold of 50% of the norm of the transition vector in the NTO basis to eliminate terms, e.g., from Eq. (9). Triplet basis states were constructed using the appropriate CSFs, as described in our previous work.[43]

Derivatives $H_{AB}^{[x]}$ were used to compute the couplings $g_{AA\theta}$ and $g_{AB\theta}$ for all phonon modes q_θ. To make contact with existing literature, we define the contributions to the relaxation energy due to the Holstein couplings, sometimes called the polaron binding energy, as

$$\epsilon_{AA\theta} = g_{AA\theta}^2/\omega_\theta. \tag{47}$$

The off-diagonal contribution to the relaxation energy, which is sometimes called the lattice distortion energy, is defined as

$$\epsilon_{AB\theta} = g_{AB\theta}^2/2\omega_\theta. \tag{48}$$

Although slightly different definitions can be found in the literature,[9] we adopt those used in Ref. 62, as we will make contact with that work in what follows. Furthermore, in the following discussion, we use the terms "relaxation energies" and "couplings" interchangeably, as the two are directly related via Eqs. (47) and (48).

IV. NUMERICAL RESULTS

Plots of the reorganization energies with the associated phonon mode frequency, as computed for the unit cell of crystalline tetracene from the PW-LDA calculations, are presented in Fig. 3. Exciton/phonon couplings for triplet exciton mobility in tetracene have not been reported previously, to the best of our knowledge, but have been reported for crystalline anthracene.[62] As these structures differ only by a single conjugated ring, we would expect some similarity with tetracene, despite the very different computational methodology that is used in Ref. 62.

For the Holstein couplings in tetracene, we find a large number of significant couplings for phonon frequencies $\omega_\theta \sim 1200$–1600 cm^{-1}, with additional significant couplings between 500 and 1000 cm^{-1}. There are essentially no Peierls couplings above ~250 cm^{-1}, and these are strongly dominated by a single coupling at the lowest-frequency mode, 53.67 cm^{-1}. Each of these observations is in excellent agreement with results for anthracene in Ref. 62. It is worth noting that the efficiency of our method allows us to compute the couplings across the whole range of phonon frequencies, and that this analysis has revealed a cluster of Holstein couplings above 3000 cm^{-1}, which is a frequency range that has not typically been investigated by others.

Where our results differ from those computed with other methods is in Holstein couplings in the lower frequency range. The presence of couplings in this region is consistent with

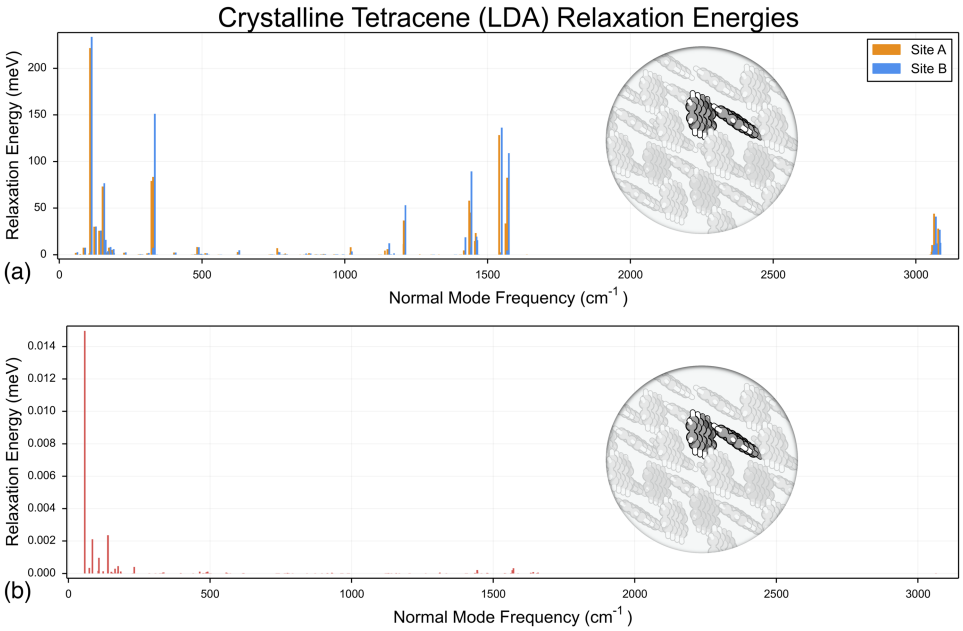

FIG. 3. Relaxation energies due to (a) local (Holstein) and (b) non-local (Peierls) couplings for crystalline tetracene, computed for the PW-LDA optimized unit cell of the "herringbone" crystal structure of tetracene. Note the significantly different vertical energy scales in the two panels.

previous work on anthracene,[62] although in the present case, the couplings are significantly more prevalent and their intensity is at least several orders of magnitude larger. A potential explanation for this discrepancy is that this is an artifact of the somewhat crude proxy for dispersion effects in the phonon mode calculations (substituting the LDA in place of a dispersion correction), as these low frequencies are primarily of intermolecular character. Grisanti *et al.* computed the intermolecular phonons using force fields instead.[62] To explore this possibility, we have performed a gas-phase optimization and frequency calculation using the dispersion-corrected ω-B97X-D functional.[68] The ωB97X-D optimized dimer exhibits a local minimum in a herringbone-type configuration that is similar to the structure of the crystalline unit cell, and we use this structure and its vibrational frequencies to compute exciton/phonon couplings, which are plotted in Fig. 4. Overall, there is a good agreement with couplings computed from the crystalline unit cell, although the couplings for the ωB97X-D structure are slightly blue-shifted in the higher-frequency region and slightly red-shifted at lower frequencies. It is also notable that the gas-phase Holstein couplings $g_{AA\theta}$ and $g_{BB\theta}$ for the dimer pair AB are nearly degenerate for the ωB97X-D geometry, for which the monomers have more flexibility to relax into similar geometries. The two Holstein couplings in each AB pair also have similar magnitudes, again suggesting that the unexpectedly large couplings in the low-frequency regime are not an artifact of the frequencies.

Grisanti *et al.* computed the Holstein couplings for anthracene using a "triplet-in-a-cluster" scheme, in which a central molecule in a cluster (taken from the crystal structure) is optimized to the triplet equilibrium geometry of the monomer,

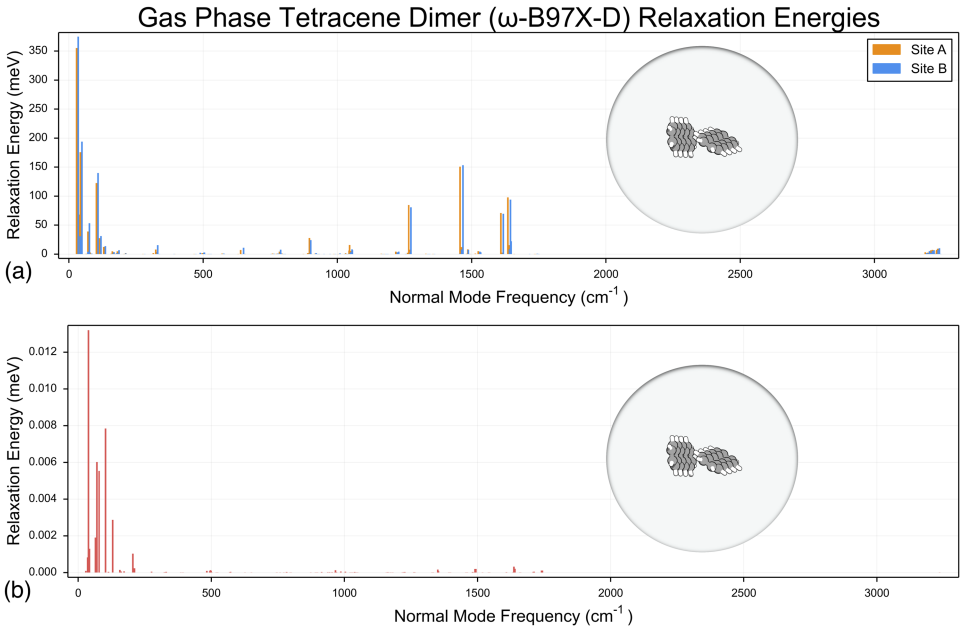

FIG. 4. Relaxation energies due to (a) local (Holstein) and (b) non-local (Peierls) couplings for the gas-phase tetracene dimer, optimized in the herringbone configuration at the ω-B97X-D/6-31+G*level.

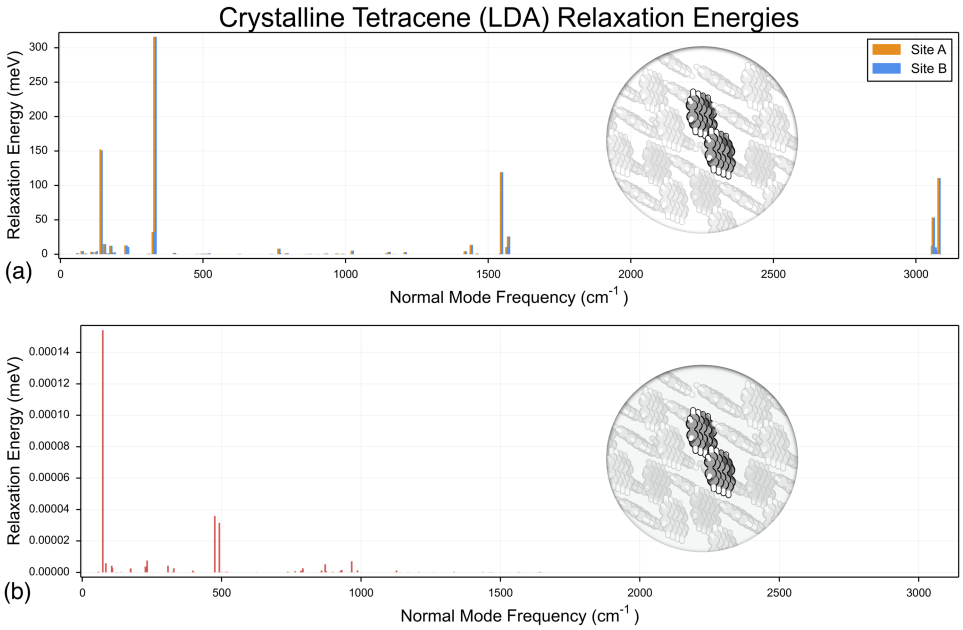

FIG. 5. Relaxation energies due to (a) local (Holstein) and (b) non-local (Peierls) couplings for crystalline tetracene computed for the parallel-stacked dimer.

in order to enforce localization of the triplet onto the central monomer.[62] (This represents a diabatization, of sorts.) Reorganization energies are then computed for the entire cluster via distortions along the phonon coordinates. With this in mind, it is not surprising that the result is couplings that are small for low-frequency phonons, as the triplet is not only in a relaxed geometry but also is free to respond to polarization induced by the vibrations. (A complete SCF calculation is performed at the perturbed geometries.) Although this scheme is certainly physically justifiable, as the intramolecular reorganization and polarization occur on much faster time scales than the intermolecular vibrations, our approach is arguably a more rigorous realization of Eq. (44) insofar as our perturbations along the phonon modes are infinitesimal. A comprehensive assessment of the relative merits of either approach is outside the scope of this work.

Thanks to the relatively low cost of our method, we can compute couplings for additional dimer configurations in order to compare pathways of mobility through the crystal. To that end, we have extracted two more dimer configurations from the crystal structure which were then also used for exciton/phonon coupling calculations. The first is a parallel-stacked configuration, and the second is a parallel but offset configuration along the long molecular axis; these will further be referred to as the stacked and offset configurations, respectively. Couplings for the stacked geometry are presented in Fig. 5 and for the offset geometry in Fig. 6. In general, the couplings for both of these configurations are quite similar, which is perhaps unsurprising as the geometries differ only by translation along a single coordinate. There is still a qualitative agreement with the "herringbone stacked" (unit cell) configuration, although both of the new configurations involve symmetric dimers, so

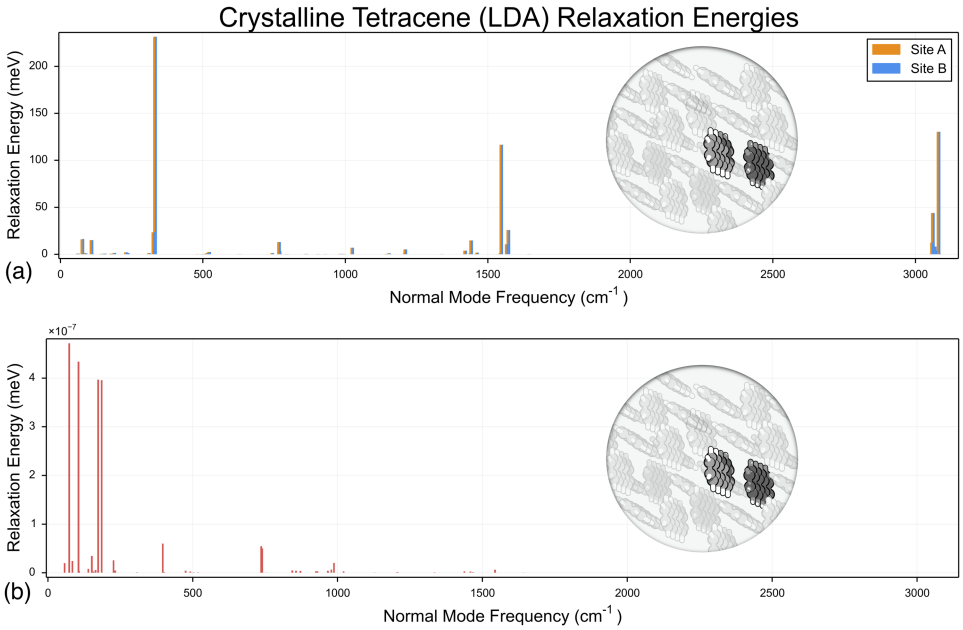

FIG. 6. Relaxation energies due to (a) local (Holstein) and (b) non-local (Peierls) couplings for crystalline tetracene, computed for the parallel-offset dimer.

TABLE II. Relaxation energies (in the tetracene unit cell geometry) for the four phonon modes identified in Ref. 43 (in the context of singlet fission) as having significant $S_1/^1(TT)$ coupling in crystalline tetracene.

Mode	ω_θ (cm^{-1})	$\epsilon_{AA\theta}$ (meV)	$\epsilon_{BB\theta}$ (meV)
127	1432.19	57.84	8.02
128	1434.08	45.10	89.32
137	1536.86	128.17	0.41
138	1539.89	2.44	136.30

the variation in frequencies and magnitudes is reduced relative to the unit cell configuration. In both cases, the strongest Holstein couplings lie around ~325 cm^{-1}, while the remaining lower-frequency couplings are significantly diminished as compared to the unit cell configuration and, in the case of the offset configuration, essentially vanish entirely. Interestingly, the couplings in the frequency range greater than 3000 cm^{-1} significantly increase in magnitude, relative to the unit cell configuration. On the other hand, the Peierls couplings decrease by two orders of magnitude for the parallel configuration and essentially vanish for offset, suggesting that these couplings play a minimal role in exciton transport outside of herringbone stacked pairs.

Recently, there has been significant interest in the nonadiabatic effects that potentially play a role in the singlet exciton fission process.[11,39,69,70] Specifically of interest are phonon modes that might modulate the crucial transition from a localized singlet exciton state to the triplet-pair intermediate. Several recent experiments[71,72] have implicated high-frequency phonon modes, in the range of ~1200–1600 cm^{-1}, as being key to the fission mechanism. It is therefore notable that we have found the exciton/phonon couplings for the triplet to be significant in this frequency range. Very recently, by utilizing AIFDEM nonadiabatic coupling calculations, we identified four high-frequency phonon modes that appear to drive the singlet fission transition in crystalline tetracene.[43] Remarkably, we have found these four modes to be significant to triplet exciton transport as well, with the corresponding Holstein couplings possessing substantial magnitude for all three crystal configurations. Reorganization energies for these modes are provided in Table II. As these modes are predominantly localized on individual monomers,[43] these couplings serve primarily to modulate the individual site energies. This correspondence suggests that the same phonon modes that induce the singlet exciton to triplet-pair transition [$S_1 \rightarrow {}^1(TT)$] also play a significant role in the subsequent transport of the free triplet excitons.

V. CONCLUSIONS

In this work, we have derived expressions for nonadiabatic derivative couplings within the theoretical framework of our novel AIFDEM excited-state method. This formalism also affords the Holstein and Peierls exciton/phonon coupling constants that are important in the description of carrier transport in solid-state semiconductors. The central task in computing these quantities is the calculation of the derivatives of the AIFDEM Hamiltonian matrix elements H_{AB} between monomers A and B, a procedure for which we have derived and implemented. As an ancillary result, we have derived expressions for derivatives of the NTO transformation and Löwdin's symmetric orthogonalization transformation, formulas for which have not previously been reported. Our implementation agrees with finite-difference results and exhibits excellent parallel scalability when matrix element derivatives are distributed across multiple cores.

We have used this new approach to compute the exciton/phonon couplings that modulate triplet exciton mobility in crystalline tetracene, comparing our results to calculations of the couplings for crystalline anthracene, performed with an entirely different computational method.[62] Mostly the agreement is quite good, with the exception of the low-frequency intermolecular Holstein couplings, for which our approach predicts significantly larger couplings as compared to Ref. 62. We conclude that the discrepancies are most likely due to methodological differences; our method computes $\partial H_{AB}/\partial x$ using analytic differentiation of rigorously defined diabatic states and is therefore free of the polarization contamination that arises in finite-displacement procedures.

Our calculations on tetracene indicate that triplet mobility is influenced by strong local couplings to intramolecular modes in the range of 1400–1600 cm^{-1} and to intermolecular modes from 50 to 300 cm^{-1}. We have also identified a cluster of local couplings >3000 cm^{-1}. The distribution of all of these local couplings remains qualitatively similar for various dimers selected from the tetracene crystal structure. The non-local couplings, on the other hand, are due entirely to low-frequency intermolecular modes <200 cm^{-1}, which vanish for any dimer configuration other than the unit cell. Four high-frequency modes that have been previously identified as "driving modes" for singlet exciton fission[43] exhibit significant couplings within this model, suggesting that the same modes that drive singlet fission may also modulate the subsequent triplet exciton transport.

VI. FUTURE WORK

The AIFDEM ansatz is flexible in that various types of basis states may be included. An obvious extension is to include charge-transfer states of the form $|\Psi_A^+\Psi_B^-\rangle$, which were included in the AIFDEM study of singlet fission in Ref. 43 but for which analytic derivatives have not yet been implemented. Such an implementation would allow us to treat couplings related to charge-carrier mobility [$^1(TT) \rightarrow T + T$]. In addition, we have previously implemented a charge-embedding scheme for the AIFDEM that significantly reduces its cost,[13] but derivatives of the charge-embedded AIFDEM have not yet been implemented. Finally, analytic derivative couplings provide analytic gradients as a special case, so that *ab initio* molecular dynamics is a possibility if the aforementioned improvements can reduce the cost sufficiently.

ACKNOWLEDGMENTS

This work was partially supported by the U.S. Department of Energy, Office of Basic Energy Sciences, Division of Chemical Sciences, Geosciences, and Biosciences under Award No.

DE-SC0008550. A.F.M. acknowledges a fellowship from the Lubrizol Corporation, and J.M.H. is a fellow of the Alexander von Humboldt Foundation. Calculations were performed at the Ohio Supercomputer Center under Project No. PAA-0003.[73] J.M.H. serves on the Board of Directors of Q-Chem, Inc.

APPENDIX: DERIVATIVE OF A SINGULAR VALUE DECOMPOSITION

This appendix provides the algorithm for taking the derivative of the SVD, adapted from Refs. 50 and 51. [A minor typographical error in Eq. (8) of Ref. 51 is also corrected here.] We use a superscript $[\gamma]$ to denote differentiation with respect to γ, but for simplicity, other indices (e.g., for monomer labels) are omitted here.

Consider a matrix function $\mathbf{A}(\gamma)$ with m rows and n columns, where m need not be equal to n. The SVD of this matrix is

$$\mathbf{A}(\gamma) = \mathbf{U}(\gamma)\,\mathbf{a}(\gamma)\,\mathbf{V}^\dagger(\gamma), \tag{A1}$$

where $\mathbf{a}(\gamma)$ is the $m \times n$ diagonal matrix of singular values, $\mathbf{U}(\gamma)$ is the $m \times m$ unitary matrix of left singular vectors, and $\mathbf{V}(\gamma)$ is the $n \times n$ unitary matrix of right singular vectors. We seek to compute derivatives of all three quantities with respect to the perturbation γ. In what follows, we suppress the explicit dependence on γ.

Differentiating Eq. (A1) affords

$$\mathbf{A}^{[\gamma]} = \mathbf{U}^{[\gamma]}\mathbf{a}\mathbf{V}^\dagger + \mathbf{U}\mathbf{a}^{[\gamma]}\mathbf{V}^\dagger + \mathbf{U}\mathbf{a}\mathbf{V}^{[\gamma]\dagger}. \tag{A2}$$

An essential detail of this algorithm is that $\mathbf{a}^{[\gamma]}$ must be diagonal, as the matrix of singular values should remain diagonal for an infinitesimal perturbation. Differentiating the unitarity condition $\mathbf{1} = \mathbf{U}^\dagger\mathbf{U}$ affords

$$\mathbf{0} = \mathbf{U}^{[\gamma]\dagger}\mathbf{U} + \mathbf{U}^\dagger\mathbf{U}^{[\gamma]} = \mathbf{Z}^\dagger + \mathbf{Z}, \tag{A3}$$

where $\mathbf{Z} = \mathbf{U}^\dagger\mathbf{U}^{[\gamma]}$. Similarly, differentiation of the condition $\mathbf{1} = \mathbf{V}^\dagger\mathbf{V}$ affords

$$\mathbf{0} = \mathbf{V}^{[\gamma]\dagger}\mathbf{V} + \mathbf{V}^\dagger\mathbf{V}^{[\gamma]} = \mathbf{W}^\dagger + \mathbf{W}, \tag{A4}$$

where $\mathbf{W} = \mathbf{V}^\dagger\mathbf{V}^{[\gamma]}$. Multiplying Eq. (A2) from the left by $\mathbf{U}^\dagger$ and from the right by $\mathbf{V}$ and rearranging affords

$$\begin{aligned}\mathbf{a}^{[\gamma]} &= \mathbf{U}^\dagger\mathbf{A}^{[\gamma]}\mathbf{V} - \mathbf{a}\mathbf{W}^\dagger - \mathbf{Z}\mathbf{a} \\ &= \mathbf{Q} - \mathbf{a}\mathbf{W}^\dagger - \mathbf{Z}\mathbf{a},\end{aligned} \tag{A5}$$

where $\mathbf{Q} = \mathbf{U}^\dagger\mathbf{A}^{[\gamma]}\mathbf{V}$. Note that both $\mathbf{Z}$ and $\mathbf{W}$ are skew-symmetric; hence, the products $\mathbf{a}\mathbf{W}^\dagger$ and $\mathbf{Z}\mathbf{a}$ are zero along the diagonal, and thus these two terms make no contribution to the singular value derivatives $\mathbf{a}^{[\gamma]}$, which are simply $a_{ii}^{[\gamma]} = Q_{ii}$.

To compute the derivatives of the singular vectors, we must solve for the elements of $\mathbf{W}$ and $\mathbf{Z}$ that force $\mathbf{a}^{[\gamma]}$ to be diagonal as specified in Eq. (A5), while enforcing skew-symmetry as specified in Eqs. (A3) and (A4). To that end, we solve $\binom{p}{2}$ systems of 2×2 equations, where $p = \min(m,n)$, each of which has the form

$$\begin{aligned}a_{kk}Z_{jk} + a_{jj}W_{kj} &= Q_{jk}, \\ a_{jj}Z_{jk} + a_{kk}W_{kj} &= -Q_{kj}.\end{aligned} \tag{A6}$$

Because $\mathbf{W}$ and $\mathbf{Z}$ are skew-symmetric, we need only to solve for either the upper or the lower triangle of each, so in Eq. (A6), we assume that $1 \le j \le \min(m,n)$ and $j < k < \min(m,n)$. Singularities may arise in solving the linear systems in Eq. (A6) when there are degeneracies amongst the singular values. The strategy in this case, as proposed in Ref. 51, is to gather sets of all 2×2 systems where $a_{jj} = a_{kk}$ and solve the systems of each set simultaneously using a least-squares approach. We use a degeneracy threshold $|a_{jj} - a_{kk}| \le 10^{-10}$.

In the case that $m \neq n$ so that $\mathbf{A}$ is rectangular, there is an additional set of equations for elements of the larger matrix,

$$\begin{aligned}a_{kk}Z_{jk} &= Q_{jk} \quad \text{if } m > n, \\ a_{kk}W_{kj} &= -Q_{kj} \text{ if } n > m.\end{aligned} \tag{A7}$$

Here $1 \le k \le \min(m,n)$ and $\min(m,n) \le j \le \max(m,n)$. Equation (A7) introduces another source of potential singularities when some a_{kk} approach zero. In our implementation, if $|a_{kk}| \le 10^{-10}$, we simply set the corresponding elements of $\mathbf{W}$ or $\mathbf{Z}$ to zero. Although not technically correct, note that we only require SVD derivatives of a rectangular matrix when computing the derivative of the NTO transformation, in which case terms associated with small singular values are neglected anyway, so this is not an issue for our use of the SVD derivative. This may not be true in general, however. In the rectangular case, if $m > n$ (or conversely $n > m$), then the triangle of Z_{jk} (or W_{kj}), where $\min(m,n) + 1 \le j \le \max(m,n)$ and $\min(m,n) + 1 \le k \le j - 1$, remains undefined, but we are free to set these elements equal to zero.[50]

Since we solve Eqs. (A6) and (A7) only for the upper triangle of $\mathbf{Z}$ and the lower triangle of $\mathbf{W}$, the final forms of $\mathbf{W}$ and $\mathbf{Z}$ are obtained from the solutions of these equations by subtracting the transpose of the solution, resulting in skew-symmetric matrices. Finally, derivatives of the singular vectors are given by

$$\begin{aligned}\mathbf{V}^{[\gamma]} &= \mathbf{V}\mathbf{W}, \\ \mathbf{U}^{[\gamma]} &= \mathbf{U}\mathbf{Z}.\end{aligned} \tag{A8}$$

[1] F. Bernardi, M. Olivucci, and M. A. Robb, Chem. Soc. Rev. **25**, 321 (1996).
[2] A. L. Sobolewski, W. Domcke, C. Dedonder-Lardeux, and C. Jouvet, Phys. Chem. Chem. Phys. **4**, 1093 (2002).
[3] B. G. Levine and T. J. Martínez, Annu. Rev. Phys. Chem. **58**, 613 (2007).
[4] W. Domcke and D. R. Yarkony, Annu. Rev. Phys. Chem. **63**, 325 (2012).
[5] S. Matsika and P. Krause, Annu. Rev. Phys. Chem. **62**, 621 (2011).
[6] J. Yang, L. Zhang, L. Wang, and D. Zhong, J. Am. Chem. Soc. **134**, 16460 (2012).
[7] G. A. Worth and L. S. Cederbaum, Annu. Rev. Phys. Chem. **55**, 127 (2004).
[8] B. E. Applegate, T. A. Barcholtz, and T. A. Miller, Chem. Soc. Rev. **32**, 38 (2003).
[9] V. Coropceanu, J. Cornil, D. A. da Silva Filho, Y. Olivier, R. Silbey, and J.-L. Brédas, Chem. Rev. **107**, 926 (2007).
[10] Y. Shu, B. S. Fales, and B. G. Levine, Nano Lett. **15**, 6247 (2015).
[11] P. M. Zimmerman, F. Bell, D. Casanova, and M. Head-Gordon, J. Am. Chem. Soc. **133**, 19944 (2011).
[12] A. F. Morrison, Z.-Q. You, and J. M. Herbert, J. Chem. Theory Comput. **10**, 5366 (2014).
[13] A. F. Morrison and J. M. Herbert, J. Phys. Chem. Lett. **6**, 4390 (2015).
[14] J. M. Herbert, X. Zhang, A. F. Morrison, and J. Liu, Acc. Chem. Res. **49**, 931 (2016).
[15] J. Frenkel, Phys. Rev. **37**, 17 (1931).
[16] A. S. Davydov, Sov. Phys. Usp. **7**, 145 (1964).
[17] B. Bouvier, T. Gustavsson, D. Markovitsi, and P. Millié, Chem. Phys. **275**, 75 (2002).
[18] B. Bouvier, J.-P. Dognon, R. Lavery, D. Markovitsi, P. Millié, D. Onidas, and K. Zakrzewska, J. Phys. Chem. B **107**, 13512 (2003).
[19] E. R. Bittner, J. Chem. Phys. **125**, 094909 (2006).

[20]A. Sisto, D. R. Glowacki, and T. J. Martinez, Acc. Chem. Res. **47**, 2857 (2014).
[21]M. J. Bearpark, M. A. Robb, and H. B. Schlegel, Chem. Phys. Lett. **223**, 269 (1994).
[22]F. Sicilia, L. Blancafort, M. J. Bearpark, and M. A. Robb, J. Chem. Theory Comput. **4**, 257 (2008).
[23]X. Zhang and J. M. Herbert, J. Chem. Phys. **141**, 064104 (2014).
[24]J. A. Kammeraad and P. M. Zimmerman, J. Phys. Chem. Lett. **7**, 5074 (2016).
[25]P. Saxe, B. H. Lengsfield III, and D. R. Yarkony, Chem. Phys. Lett. **113**, 159 (1985).
[26]B. H. Lengsfield III and D. R. Yarkony, J. Chem. Phys. **84**, 348 (1986).
[27]B. H. Lengsfield III, P. Saxe, and D. R. Yarkony, J. Chem. Phys. **81**, 4549 (1984).
[28]H. Lischka, M. Dallos, P. G. Szalay, D. R. Yarkony, and R. Shepard, J. Chem. Phys. **120**, 7322 (2004).
[29]I. F. Galván, M. G. Delcey, T. B. Pedersen, F. Aquilante, and R. Lindh, J. Chem. Theory Comput. **12**, 3636 (2016).
[30]O. Christiansen, J. Chem. Phys. **110**, 711 (1999).
[31]A. Tajti and P. G. Szalay, J. Chem. Phys. **131**, 124104 (2009).
[32]S. Fatehi, E. Alguire, Y. Shao, and J. E. Subotnik, J. Chem. Phys. **135**, 234105 (2011).
[33]S. Fatehi and J. E. Subotnik, J. Phys. Chem. Lett. **3**, 2039 (2012).
[34]X. Zhang and J. M. Herbert, J. Chem. Phys. **142**, 064109 (2015).
[35]R. Send and F. Furche, J. Chem. Phys. **132**, 044107 (2010).
[36]Z. Li, B. Suo, and W. Liu, J. Chem. Phys. **141**, 244105 (2014).
[37]Q. Ou, G. D. Bellchambers, F. Furche, and J. E. Subotnik, J. Chem. Phys. **142**, 064114 (2015).
[38]F. Liu, Z. Gan, Y. Shao, C.-P. Hsu, A. Dreuw, M. Head-Gordon, B. T. Miller, B. R. Brooks, J.-G. Yu, T. R. Furlani, and J. Kong, Mol. Phys. **108**, 2791 (2010).
[39]X. Feng, A. V. Luzanov, and A. I. Krylov, J. Phys. Chem. Lett. **4**, 3845 (2013).
[40]A. V. Luzanov, A. A. Sukhorukov, and V. E. Umanskii, Theor. Exp. Chem. **10**, 354 (1974).
[41]R. L. Martin, J. Chem. Phys. **118**, 4775 (2003).
[42]I. Mayer, Chem. Phys. Lett. **437**, 284 (2007).
[43]A. F. Morrison and J. M. Herbert, J. Phys. Chem. Lett. **8**, 1442 (2017).
[44]D. Maurice and M. Head-Gordon, Mol. Phys. **96**, 1533 (1999).
[45]S. Hirata and M. Head-Gordon, Chem. Phys. Lett. **314**, 291 (1999).
[46]P. R. Surján, Chem. Phys. Lett. **439**, 393 (2007).
[47]A. T. Amos and G. G. Hall, Proc. R. Soc. A **263**, 483 (1961).
[48]H. F. King, R. E. Stanton, H. Kim, R. E. Wyatt, and R. G. Parr, J. Chem. Phys. **47**, 1936 (1967).
[49]A. J. W. Thom and M. Head-Gordon, J. Chem. Phys. **131**, 124113 (2009).
[50]K. Wright, Numer. Math. **63**, 283 (1992).
[51]T. Papadopoulo and M. I. A. Lourakis, "Estimating the Jacobian of the singular value decomposition: Theory and applications," in *Proceedings of the 6th European Conference on Computer Vision—Part I (ECCV '00)*, edited by D. Vernon (Springer-Verlag, London, UK, 2000), pp. 554–570.
[52]J. A. Pople, R. Krishnan, H. B. Schlegel, and J. S. Binkley, Int. J. Quantum Chem. Symp. **16**, 225 (1979).
[53]N. C. Handy and H. F. Schaefer III, J. Chem. Phys. **81**, 5031 (1984).
[54]K. Hannewald and P. A. Bobbert, Appl. Phys. Lett. **85**, 1535 (2004).
[55]A. Troisi and G. Orlandi, Phys. Rev. Lett. **96**, 086601 (2006).
[56]A. Troisi, Adv. Mater. **19**, 2000 (2007).
[57]A. Girlando, L. Grisanti, M. Masino, I. Bilotti, A. Brillante, R. G. Della Valle, and E. Venuti, Phys. Rev. B **82**, 035208 (2010).
[58]T. Kato and T. Yamabe, J. Chem. Phys. **115**, 8592 (2001).
[59]A. Troisi and G. Orlandi, J. Phys. Chem. A **110**, 4065 (2006).
[60]A. Painelli and A. Girlando, J. Chem. Phys. **84**, 5655 (1986).
[61]E. B. Wilson, J. C. Decius, and P. C. Cross, *Molecular Vibrations: The Theory of Infrared and Raman Vibrational Spectra* (McGraw-Hill, 1955).
[62]L. Grisanti, Y. Olivier, L. Wang, S. Athanasopoulos, J. Cornil, and D. Beljonne, Phys. Rev. B **88**, 035450 (2013).
[63]Y. Shao, Z. Gan, E. Epifanovsky, A. T. B. Gilbert, M. Wormit, J. Kussmann, A. W. Lange, A. Behn, J. Deng, X. Feng, D. Ghosh, M. Goldey, P. R. Horn, L. D. Jacobson, I. Kaliman, R. Z. Khaliullin, T. Kús, A. Landau, J. Liu, E. I. Proynov, Y. M. Rhee, R. M. Richard, M. A. Rohrdanz, R. P. Steele, E. J. Sundstrom, H. L. Woodcock III, P. M. Zimmerman, D. Zuev, B. Albrecht, E. Alguire, B. Austin, G. J. O. Beran, Y. A. Bernard, E. Berquist, K. Brandhorst, K. B. Bravaya, S. T. Brown, D. Casanova, C.-M. Chang, Y. Chen, S. H. Chien, K. D. Closser, D. L. Crittenden, M. Diedenhofen, R. A. DiStasio, Jr., H. Dop, A. D. Dutoi, R. G. Edgar, S. Fatehi, L. Fusti-Molnar, A. Ghysels, A. Golubeva-Zadorozhnaya, J. Gomes, M. W. D. Hanson-Heine, P. H. P. Harbach, A. W. Hauser, E. G. Hohenstein, Z. C. Holden, T.-C. Jagau, H. Ji, B. Kaduk, K. Khistyaev, J. Kim, J. Kim, R. A. King, P. Klunzinger, D. Kosenkov, T. Kowalczyk, C. M. Krauter, K. U. Lao, A. Laurent, K. V. Lawler, S. V. Levchenko, C. Y. Lin, F. Liu, E. Livshits, R. C. Lochan, A. Luenser, P. Manohar, S. F. Manzer, S.-P. Mao, N. Mardirossian, A. V. Marenich, S. A. Maurer, N. J. Mayhall, C. M. Oana, R. Olivares-Amaya, D. P. O'Neill, J. A. Parkhill, T. M. Perrine, R. Peverati, P. A. Pieniazek, A. Prociuk, D. R. Rehn, E. Rosta, N. J. Russ, N. Sergueev, S. M. Sharada, S. Sharmaa, D. W. Small, A. Sodt, T. Stein, D. Stück, Y.-C. Su, A. J. W. Thom, T. Tsuchimochi, L. Vogt, O. Vydrov, T. Wang, M. A. Watson, J. Wenzel, A. White, C. F. Williams, V. Vanovschi, S. Yeganeh, S. R. Yost, Z.-Q. You, I. Y. Zhang, X. Zhang, Y. Zhou, B. R. Brooks, G. K. L. Chan, D. M. Chipman, C. J. Cramer, W. A. Goddard III, M. S. Gordon, W. J. Hehre, A. Klamt, H. F. Schaefer III, M. W. Schmidt, C. D. Sherrill, D. G. Truhlar, A. Warshel, X. Xua, A. Aspuru-Guzik, R. Baer, A. T. Bell, N. A. Besley, J.-D. Chai, A. Dreuw, B. D. Dunietz, T. R. Furlani, S. R. Gwaltney, C.-P. Hsu, Y. Jung, J. Kong, D. S. Lambrecht, W. Liang, C. Ochsenfeld, V. A. Rassolov, L. V. Slipchenko, J. E. Subotnik, T. Van Voorhis, J. M. Herbert, A. I. Krylov, P. M. W. Gill, and M. Head-Gordon, Mol. Phys. **113**, 184 (2015).
[64]P. Giannozzi, S. Baroni, N. Bonini, M. Calandra, R. Car, C. Cavazzoni, D. Ceresoli, G. L. Chiarotti, M. Cococcioni, I. Dabo, A. Dal Corso, S. de Gironcoli, S. Fabris, G. Fratesi, R. Gebauer, U. Gerstmann, C. Gougoussis, A. Kokalj, M. Lazzeri, L. Martin-Samos, N. Marzari, F. Mauri, R. Mazzarello, S. Paolini, A. Pasquarello, L. Paulatto, C. Sbraccia, S. Scandolo, G. Sclauzero, A. P. Seitsonen, A. Smogunov, P. Umari, and R. M. Wentzcovitch, J. Phys.: Condens. Matter **21**, 395502 (2009).
[65]D. Holmes, S. Kumaraswamy, A. J. Matzger, and K. P. C. Vollhardt, Chem. - Eur. J. **5**, 3399 (1999).
[66]D. Holmes, S. Kumaraswamy, A. J. Matzger, and K. P. C. Vollhardt, CCDC 114446: Experimental crystal structure determination, 1999, deposited on: 8/2/1999.
[67]M. Abdulla, K. Refson, R. H. Friend, and P. D. Haynes, J. Phys.: Condens. Matter **27**, 375402 (2015).
[68]J.-D. Chai and M. Head-Gordon, Phys. Chem. Chem. Phys. **10**, 6615 (2008).
[69]R. W. A. Havenith, H. D. de Gier, and R. Broer, Mol. Phys. **110**, 2445 (2012).
[70]T. C. Berkelbach, M. S. Hybertsen, and D. R. Reichman, J. Chem. Phys. **138**, 114103 (2013).
[71]A. J. Musser, M. Liebel, C. Schnedermann, T. Wende, T. B. Kehoe, A. Rao, and P. Kukura, Nat. Phys. **11**, 352 (2015).
[72]A. A. Bakulin, S. E. Morgan, T. B. Kehoe, M. W. B. Wilson, A. W. Chin, D. Zigmantas, D. Egorova, and A. Rao, Nat. Chem. **8**, 16 (2016).
[73]See http://osc.edu/ark:/19495/f5s1ph73 for Ohio Supercomputer Center.